

# A design procedure for subscale airfoils with full-scale leading edges for ice accretion testing

**Farooq Saeed**

*Illinois Univ., Urbana*

**Michael S. Selig**

*Illinois Univ., Urbana*

**Michael B. Bragg**

*Illinois Univ., Urbana*

**AIAA 34th Aerospace Sciences Meeting and Exhibit, Reno, NV Jan 15-18, 1996**

A design procedure for subscale airfoils with full-scale leading edges that exhibit full-scale water droplet impingement characteristics in an incompressible inviscid flow is presented. The design procedure uses validated airfoil design, flow analysis, and water droplet impingement simulation codes to accomplish the task. To identify and isolate important design variables in the design, numerous trade studies were performed. The paper presents the results of the trade studies and briefly discusses the role of important design variables in the subscale airfoil design. The effect of these design variables on circulation, velocity distribution, and impingement characteristics is discussed along with the accompanying implications and compromises in the design. A strategy to incorporate viscous effects into the design is also presented. This paper also presents the design of a half-scale airfoil model with a 5-percent upper and 20-percent lower full-scale surface of the Learjet 305 airfoil leading-edge and compares its aerodynamic, as well as the droplet impingement, characteristics with that of the Learjet 305 airfoil. (Author)

## A DESIGN PROCEDURE FOR SUBSCALE AIRFOILS WITH FULL-SCALE LEADING EDGES FOR ICE ACCRETION TESTING

Farooq Saeed,\* Michael S. Selig† and Michael B. Bragg‡  
 Department of Aeronautical and Astronautical Engineering  
 University of Illinois at Urbana-Champaign  
 Urbana, Illinois 61801

### ABSTRACT

A design procedure for subscale airfoils with full-scale leading edges that exhibit full-scale water droplet impingement characteristics in an incompressible, inviscid flow is presented. The design procedure uses validated airfoil design, flow analysis and water droplet impingement simulation codes to accomplish the task. To identify and isolate important design variables in the design, numerous trade studies were performed. The paper presents the results of the trade studies and briefly discusses the role of important design variables in the subscale airfoil design. The effect of these design variables on circulation, velocity distribution and impingement characteristics is discussed along with the accompanying implications and compromises in the design. A strategy to incorporate viscous effects into the design is also presented. The paper also presents the design of a half-scale airfoil model with a 5% upper and 20% lower full-scale surface of the Learjet 305 airfoil leading-edge and compares its aerodynamic as well as the droplet impingement characteristics with that of the Learjet 305 airfoil.

### NOMENCLATURE

$c$  = airfoil chord length  
 $C_d$  = airfoil drag coefficient  
 $C_l$  = airfoil lift coefficient  
 $c_{mo}$  = airfoil pitching moment coefficient  
 $F_r$  = Froude number,  $U/\sqrt{cg}$   
 $K$  = droplet inertia parameter,  $\rho_w \delta^2 U / 18c\mu$   
 $K_S$  = trailing-edge thickness parameter  
 $M$  = freestream Mach number  
 $Re$  = freestream Reynolds number,  $\rho U c / \mu$   
 $Re_U$  = droplet freestream Reynolds number,  $\rho \delta U / \mu$   
 $S$  = airfoil surface arc length measured from the leading-edge

$T$  = freestream static temperature  
 $u, v$  = local flowfield horizontal and vertical velocity components  
 $U$  = freestream velocity  
 $V$  = surface velocity  
 $VMD$  = volume median droplet diameter  
 $x, y$  = airfoil coordinates  
 $x_o, y_o$  = initial horizontal and vertical displacement of the droplet  
 $x_m, \bar{x}_m$  = upper and lower surface match locations  
 $x_r, \bar{x}_r$  = upper and lower surface pressure recovery locations  
 $v_1$  = design velocity level for segment 1  
 $\alpha$  = angle of attack relative to the chord line  
 $\alpha_e$  = effective angle of attack relative to the nose section chord line,  $\alpha - \gamma$   
 $\alpha^*, \bar{\alpha}^*$  = upper and lower surface multipoint design angle of attack distribution  
 $\beta$  = local impingement efficiency  
 $\phi_{le}$  = leading-edge arc limit  
 $\gamma$  = nose droop angle  
 $\Gamma$  = circulation strength normalized by  $Uc$   
 $\bar{\Gamma}$  = circulation strength,  $m^2/s$   
 $\delta$  = droplet diameter  
 $\eta$  = normalized subscale airfoil chord length,  $c_{ss}/c_{fs}$   
 $\mu$  = air viscosity  
 $\rho$  = air density  
 $\rho_w$  = water density  
 $\tau$  = finite trailing-edge angle

**Subscripts:**  
 $fs$  = full-scale airfoil  
 $i$  = inviscid  
 $l$  = lower surface  
 $ss$  = subscale airfoil  
 $u$  = upper surface  
 $v$  = viscous

### INTRODUCTION

Recent aircraft accidents have raised important flight safety issues related to the effect of ice accretion on airfoil and wing performance. In order to improve flight safety, a better understanding of the effect of ice accretion on the aerodynamic performance of modern airfoils is required. One important step in this process is to evaluate the aerodynamic performance of the airfoil sections (or the wing as a

Copyright © 1996 by Farooq Saeed, Michael S. Selig and Michael B. Bragg. Published by the American Institute of Aeronautics and Astronautics, Inc. with permission.

\* Graduate Research Assistant. Student Member AIAA.

† Assistant Professor. Member AIAA.

‡ Professor. Associate Fellow AIAA.

whole) at the icing conditions within the certification icing envelop that result in the largest performance penalties.

Since ice accretion scaling is still not well understood, testing at full-scale or near full-scale conditions is highly desirable. The available ice accretion tunnels, however, are too small to test full-scale airfoils or wings of most aircraft of interest. Numerous investigators have performed experimental or analytical studies<sup>1-4</sup> in an effort to evaluate full-scale icing protection systems for wing sections using truncated airfoil models. These truncated airfoil models utilize a full-scale leading edge section followed by a faired or flapped aft section that, in effect, reduces the overall length or chord of the model. To our knowledge, however, no systematic study has been performed to provide insight into the design of the aft section.

With these issues in mind, a subscale model design procedure was formulated with the objective of providing design guidance for subscale models that simulate full-scale water droplet impingement characteristics. It is assumed that ice accretion will be the same if droplet impingement, surface geometry and surface flowfield are the same provided the same cloud properties, model surface quality, model surface thermodynamic characteristics exist. Using the fact that ice usually accretes only on the airfoil leading edge, where the supercooled water droplets impinge and form ice, the subscale airfoil model is designed with a leading-edge geometry (first 10-20% of chord) identical to that of the full-scale leading edge. The design of the aft section is such that it provides full-scale flowfield and droplet impingement on the leading edge. Using this formulation, the effect of various design variables on the inviscid flowfield and droplet impingement characteristics of the subscale airfoil was examined to obtain useful guidelines for the design. The final design is based on viscous considerations as well.

The model design procedure for full-scale flowfield and droplet impingement simulation uses validated computational airfoil aerodynamics and droplet impingement codes,<sup>5-15</sup> specifically, an inverse design method,<sup>10</sup> the Eppler code,<sup>8,9</sup> XFOIL<sup>11</sup> and AIRDROP.<sup>12</sup>

## DESIGN APPROACH

A conceptual illustration of the subscale airfoil design procedure is shown in Fig. 1. First, a droplet impingement code can be used to predict the limits of the droplet impingement, which defines the initial ice accretion envelop. (The droplet impingement code, AIRDROP,<sup>12</sup> is discussed later.) Once

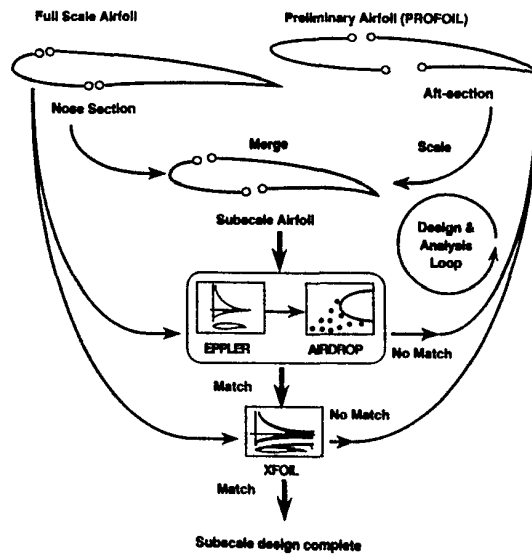


Fig. 1 A conceptual illustration of the subscale airfoil design procedure.

the limits of impingement are known over the leading edge of the full-scale airfoil, that part of the full-scale airfoil geometry is fixed for the subsequent subscale airfoil shapes. For the sake of discussion, this fixed leading-edge section, which is common to both the full scale airfoil and the subscale airfoil, is referred to as the nose section while the remaining section of the subscale airfoil profile is referred to as the aft section. The aft section of the subscale airfoil is then designed to provide full-scale flowfield and droplet impingement on the nose section of the subscale airfoil.

An initial geometry for the aft section is obtained through the use of a multipoint inverse airfoil design code<sup>10</sup> (PROFOIL). The design of this intermediate airfoil, from which the aft section of the subscale airfoil is derived, is governed by several constraints, namely, the scale of the subscale airfoil, the upper and lower surface thickness and slope at the junction between the nose and aft sections ( $x_m$ ,  $\bar{x}_m$ ), and a desired form for the pressure recovery characteristics. Apart from these constraints, additional continuity and closure constraints that form an integral part of the inverse design methodology<sup>10</sup> are also satisfied in order to achieve a physically possible design. A multi-dimensional Newton iteration scheme is employed to satisfy these constraints. The dependent and independent Newton variables<sup>10</sup> used in the design are listed Table 1. Once the constraints are satisfied, the aft section is combined with the nose section to form a subscale airfoil.

The potential flow over both the subscale and the full-scale airfoils is then analyzed using the

**Table 1 Newton variables used in the design.**

Dependent Variables	Independent Variables
$K_S = 0.3$	$\phi_{lc}$
$c_{m_o}$	$v_1$
$y(x_m)$	$\alpha^*$
$y(\bar{x}_m)$	$\bar{\alpha}^*$

Eppler code, which has the capability to analyze the potential flow over the airfoils using a method that employs panels with distributed surface singularities. The singularities used are vorticities distributed parabolically along each panel. Results predicted by the Eppler code have been shown to compare well with experiments.<sup>16,17</sup>

In order to have a physically similar flow in the vicinity of the nose section of both the subscale and the full-scale airfoils, the analysis is performed at the same angle of attack relative to the nose section chord of both the airfoils. The local inviscid velocity distributions over the nose section and the stagnation point locations on both the subscale and full-scale airfoils are then compared. If the desired velocity distribution over the nose section and stagnation point location are not achieved, the aft section of the subscale airfoil is redesigned and again merged with the nose section to form a new subscale airfoil. The flow over the new subscale airfoil is then analyzed and compared with that over the full scale airfoil. The process is repeated until the desired inviscid velocity distribution over the nose section and the stagnation point location are achieved.

In the next step, the subscale airfoil circulation, water droplet trajectories and water droplet impingement characteristics are determined from AIRDROP. The airfoil droplet impingement code, AIRDROP, written by Bragg<sup>12</sup> predicts droplet trajectories and the resultant impingement efficiency on single element airfoils in incompressible flow. The code has been validated against NACA airfoil droplet impingement data and compares well when the cloud droplet size distribution is modeled correctly and the code is run matching the airfoil lift coefficient.<sup>12</sup> Comparisons with predicted and measured rime ice accretion show good agreement.

The numerical procedure employed by AIRDROP consists of two steps. First, the flowfield around the airfoil is determined by Woan's method.<sup>18</sup> Second, single water droplet trajectories are calculated from the trajectory equation,<sup>12</sup> which in nondimensional form contains the three additional similarity parameters  $R_U$ ,  $F_r$  and  $K$ , apart from  $Re$  and  $M$ . Thus, given  $R_U$ ,  $F_r$ ,  $K$ , the droplet initial location, and the airfoil geometry, single water droplet trajectories are

determined from the trajectory equation.<sup>12</sup>

The individual droplet trajectories are combined to calculate the local impingement efficiency  $\beta$  ( $= dy_o/dS$ ). The impingement efficiency represents the dimensionless mass flux of impinging droplets at a point on the airfoil. Here,  $y_o$  is the initial  $y$  displacement of an impinging droplet far ahead ( $x_o = -5c_{fs}$ ) of the airfoil, and  $S$  is the surface length of the impact location measured from the leading edge of the airfoil. The AIRDROP code calculates a series of droplet trajectories, fits a cubic spline through the  $y_o$  vs  $S$  data points of the impinging droplets, and then computes the slope of the spline at a series of surface positions. This slope is  $\beta$  at that surface location. In this paper, the  $y_o$  vs  $S$  plot is referred to as the  $y_o$ -curve and the  $\beta$  vs  $S$  plot is referred to as the  $\beta$ -curve. And the term "impingement characteristics" refers to both the  $y_o$ -curve and  $\beta$ -curve.

The impingement characteristics of both the full scale and subscale airfoil are then compared with each other. If the agreement in the impingement characteristics is poor, the subscale airfoil is modified and the design process is repeated again until a good agreement is reached.

As will be shown later, the amount of circulation plays a dominant role in determining the impingement characteristics through its impact on the flowfield droplet trajectories ( $y_o$ -curve). The expression for the total circulation can be derived from the relation

$$L = \rho U \bar{\Gamma} = \frac{1}{2} \rho U^2 c C_l \quad (1)$$

which yields

$$\bar{\Gamma} = \frac{\Gamma}{U c} = \frac{1}{2} C_l \quad (2)$$

Therefore, the full-scale and subscale airfoil circulation is,

$$\Gamma_{fs} = \frac{1}{2} C_{l,fs}, \quad \Gamma_{ss} = \frac{\eta}{2} C_{l,ss} \quad (3,4)$$

respectively, where  $\eta$  is the normalized subscale airfoil chord length.

Finally, in order to obtain a physically realistic subscale airfoil design, consideration must also be given to viscous and compressibility effects to determine the true merits of the design. A discussion of the viscous considerations is presented in a later section.

## IMPLEMENTATION

To expedite the design procedure, the Eppler code, PROFOIL, and AIRDROP were integrated

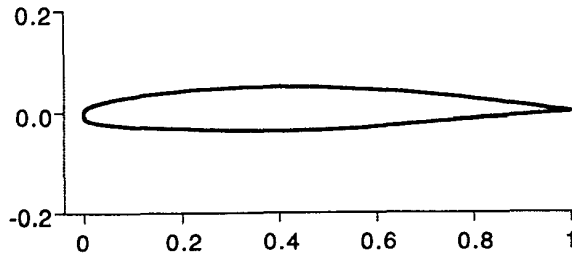


Fig. 2 The Learjet 305 (GLC 305) airfoil.

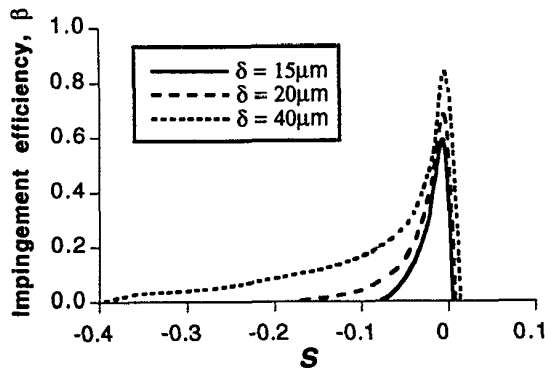


Fig. 3 Droplet impingement efficiency predicted by AIRDROP for the Learjet 305 airfoil.

into a single computer program. Then, the constraints on the subscale airfoil design were defined in terms of the fixed nose section geometry, velocity distribution over the nose section, total circulation and the angle of attack relative to the nose section of a full-scale airfoil. In order to satisfy all of the above constraints, numerous parametric trade studies were performed to help identify and isolate various key independent design variables. These independent variables were later identified as the pitching moment coefficient  $c_{m_0}$  of the airfoil from which the aft section of the subscale airfoil is derived, the scale  $\eta$  of the subscale airfoil, the nose droop angle  $\gamma$ , and the upper and lower surface pressure recovery locations  $x_r$  and  $\bar{x}_r$ .

To illustrate the effects of the independent design variables on the subscale airfoil design, the Learjet 305 (GLC 305) airfoil, shown in Fig. 2, was selected as the full-scale airfoil along with the flight and icing conditions listed in Table 2. At these conditions for the GLC 305 airfoil, AIRDROP predicts a lift coefficient  $C_{l,f_s} = 0.736$  and the circulation  $\Gamma_{f_s} = 0.368$ . Figure 3 shows the corresponding  $\beta$ -curves as predicted by AIRDROP. For  $VMD = 20\mu\text{m}$ , AIRDROP predicts the maximum limits of impingement as  $S_u = 0.0076$  ( $x/c = 0.0019$ ) on the upper surface and  $S_l = -0.1822$  ( $x/c = 0.1738$ ) on the lower surface.

Table 2 Typical Flight and Icing conditions.

Airspeed, $U$	= 87 m/s (175 kt)
Static temperature, $T$	= -5 deg C
Reynolds number, $Re$	= $6 \times 10^6$
Mach number, $M$	= 0.28
$VMD$	= 15-40 $\mu\text{m}$
Angle of attack, $\alpha$	= 6 deg

Since the limits of impingement define the surface within which ice will accrete on the airfoil, only that part of the full scale geometry need be fixed as the nose section for the subscale airfoil. The nose section size is kept to a minimum, thereby, allowing more flexibility in the design of the aft section to satisfy the constraints. Thus, the nose section geometry was selected as the full scale airfoil surface from  $x/c = 0.05$  on the upper surface to  $x/c = 0.20$  on the lower surface. Moreover, a half-scale ( $\eta = 0.5$ ) subscale model was selected as the baseline case. Based on the size of droplets under consideration, the effect of gravity on the droplets was considered negligible and, therefore, was ignored.

Most of the important effects can be examined by only considering inviscid effects; that is, boundary-layer displacement effects are second order relative to the effects of pitching moment, subscale airfoil chord length and the nose droop. Thus the remainder of this section is divided into inviscid and viscous considerations.

### Inviscid Considerations

#### Effect of Pitching Moment Coefficient ( $c_{m_0}$ )

The effect of the pitching moment coefficient is illustrated in Fig. 4, in which, an increase in the pitching moment coefficient  $c_{m_0}$  (more negative) results in a subscale airfoil with a greater aft camber and, therefore, a higher aft loading as well as an increase in the amount of circulation. The change in circulation with  $c_{m_0}$  is found to be nearly linear. The droplet impingement characteristics, specifically the  $y_o$ -curves, also indicate a strong dependence on the value of circulation which makes the pitching moment coefficient  $c_{m_0}$  the main independent design variable (Note that,  $c_{m_0}$  assumes a role of a dependent design variable in the design of the aft section). Figure 4(d) indicates that the subscale airfoil requires slightly less circulation (by 4.5%) than the full scale airfoil to achieve full-scale droplet impingement. One explanation is that the subscale airfoil is able to achieve full-scale droplet impingement with slightly less circulation due to the distribution of vorticity. In the case of a subscale airfoil the vorticity is more "concentrated" near the leading-edge than in the case of the full scale airfoil resulting in



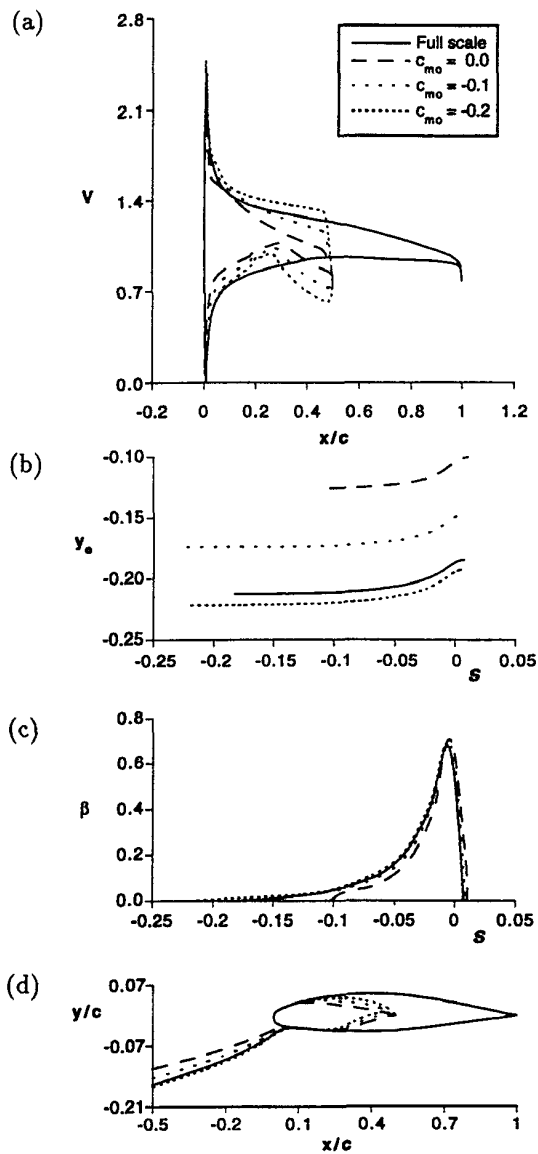


Fig. 4 The effect of pitching moment coefficient on (a) the velocity distribution, (b) initial displacement, (c) droplet impingement efficiency and (d) the tangent droplet trajectories.

a greater upwash in close proximity of the airfoil. Thus a lower value of overall circulation is required to simulate full scale droplet impingement.

#### Effect of Chord Length ( $\eta$ )

To examine the effect of normalized subscale chord length  $\eta$  on the design, subscale airfoils were designed for three different values of  $\eta$ , that is, 0.5, 0.7 and 0.9. Initially, the three subscale airfoils were designed such that they produced the same amount of circulation as the full scale airfoil. Figure

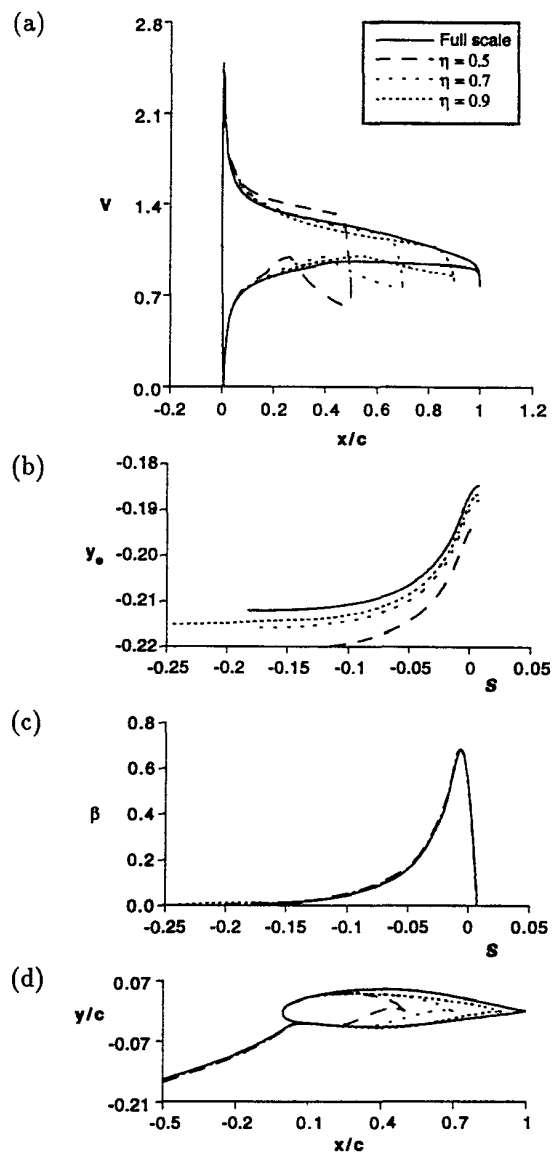


Fig. 5 The effect of chord length on (a) the velocity distribution, (b) initial displacement, (c) droplet impingement efficiency and (d) the tangent droplet trajectories.

5 shows the resulting velocity distribution impingement characteristics and the airfoil shapes. The results indicate that as the scale of the subscale model is reduced, the aft-loading on the airfoil increases significantly in order for it to produce the same amount of circulation. The mismatch in the  $y_o$ -curves, Fig. 5(b), suggests that subscale models require less circulation to achieve full scale impingement characteristics. Moreover, the results also suggest that the smaller the scale, the less circulation required to simulate full scale droplet impingement

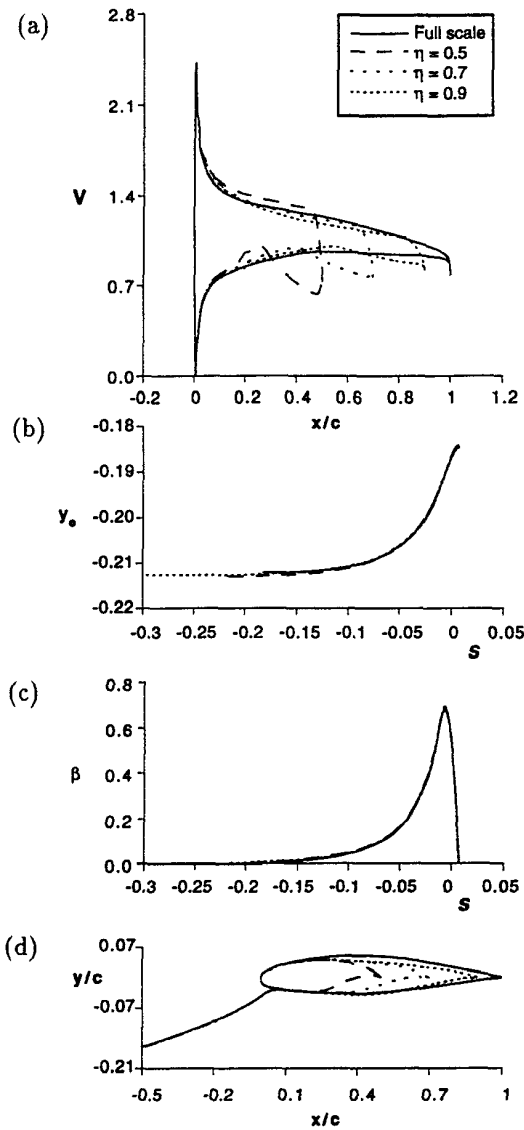


Fig. 6 Results showing (a) the velocity distribution, (b) initial displacement, (c) droplet impingement efficiency and (d) the tangent droplet trajectories at the matched conditions.

characteristics. The subscale airfoils shown in Fig. 6 were designed such that the impingement characteristics, specifically, the  $y_0$ -curves were matched. The match in  $y_0$ -curves was achieved by designing subscale airfoils with reduced circulation as compared with the ones in Fig. 5. The results also indicate that the amount of circulation required to simulate full scale droplet impingement vary from  $(0.955\Gamma_{fs})$  for  $\eta$  of 0.5 to  $(0.983\Gamma_{fs})$  for  $\eta$  of 0.9.

#### Effect of Nose Droop Angle ( $\gamma$ )

The effect of the nose droop angle  $\gamma$ , shown in Fig. 7, becomes obvious from Fig. 8 which illustrates

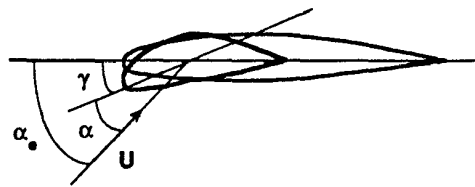


Fig. 7 The nose droop angle.

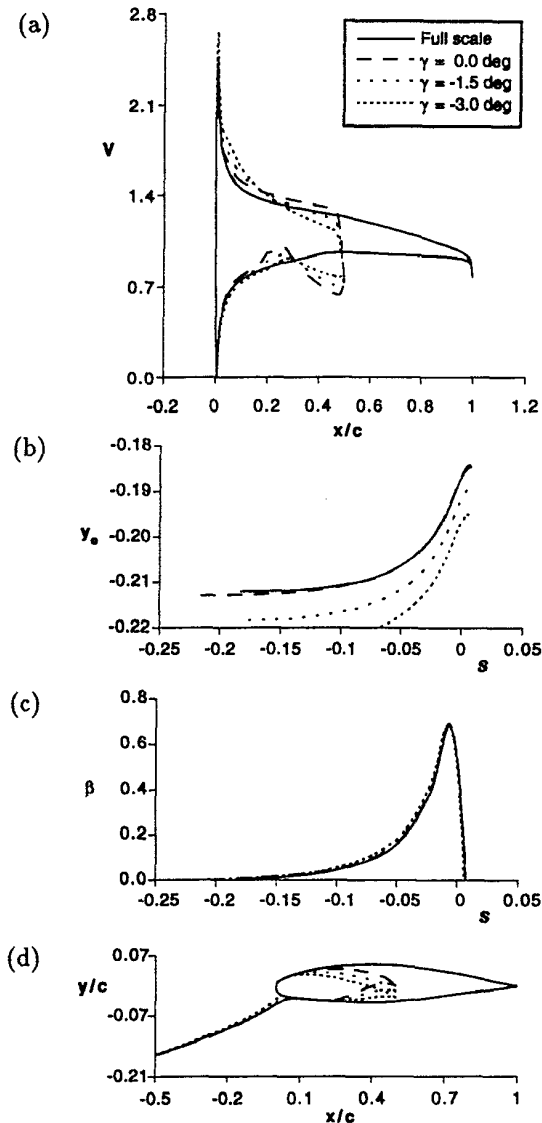


Fig. 8 The effect of nose droop on (a) the velocity distribution, (b) initial displacement, (c) droplet impingement efficiency and (d) the tangent droplet trajectories.

the usefulness of the nose droop in reducing the high aft-loading on airfoils. In order to keep the angle of attack relative to the nose section chord constant

for both the full scale and subscale airfoils, the subscale airfoil with a nose droop is analyzed at an effective angle of attack  $\alpha_e$  which takes into account the nose droop angle. As a result, the subscale airfoils with nose sections droop downwards are analyzed at higher angles of attack than those without the nose droop. Figure 8 shows the results of the subscale airfoil design with different nose droop angles for the same value of circulation as that of the half-scale model without the nose droop. The results indicate that the nose droop results in an increase in the camber of the subscale airfoil and, therefore, the subscale airfoil circulation. Moreover, the subscale airfoils with the nose drooped downwards also operate at higher absolute angles of attack defined by  $\alpha_e$ . As a result of this increase, the impingement characteristics show a mismatch. By decreasing the amount of circulation by an appropriate amount, the mismatch was removed as shown in Fig. 9. The reduction in the value of circulation as compared with that for the full scale airfoil varies from  $(0.955\Gamma_{fs})$  for  $\gamma$  of 0 deg to  $(0.892\Gamma_{fs})$  for  $\gamma$  of -3 deg.

#### Other Effects

The upper and lower surface pressure recovery locations  $x_r$  and  $\bar{x}_r$  (see Fig. 10) control to a great extent the shape of the airfoil near its trailing edge. Although, the effect of moving the pressure recovery locations  $x_r$  and  $\bar{x}_r$  results in a significant amount of improvement in the velocity distributions and ultimately the viscous characteristics, the change in the droplet impingement characteristics is, however, small.

The above study, based on inviscid considerations alone, illustrates the effect of different independent design variables on the subscale airfoil design. The results indicate that subscale airfoils require less circulation to simulate full scale airfoil droplet impingement characteristics. The pitching moment coefficient  $c_{mo}$  can be used effectively to achieve the desired amount of circulation. Since subscale airfoils tend toward high aft-loading in order to simulate the desired impingement characteristics, a nose droop can be used effectively to offset the high aft-loading to a large extent. The above study also reveals that subscale airfoils with a nose droop require even less circulation to achieve the desired impingement characteristics. Moreover, a subscale airfoil with a nose droop (downwards) must operate at a higher absolute angle of attack to simulate full scale impingement characteristics over its nose section. Operation at high absolute angles of attack makes the subscale airfoil highly susceptible to flow separation and, therefore, it becomes necessary to evaluate the performance by means of a viscous analysis of the

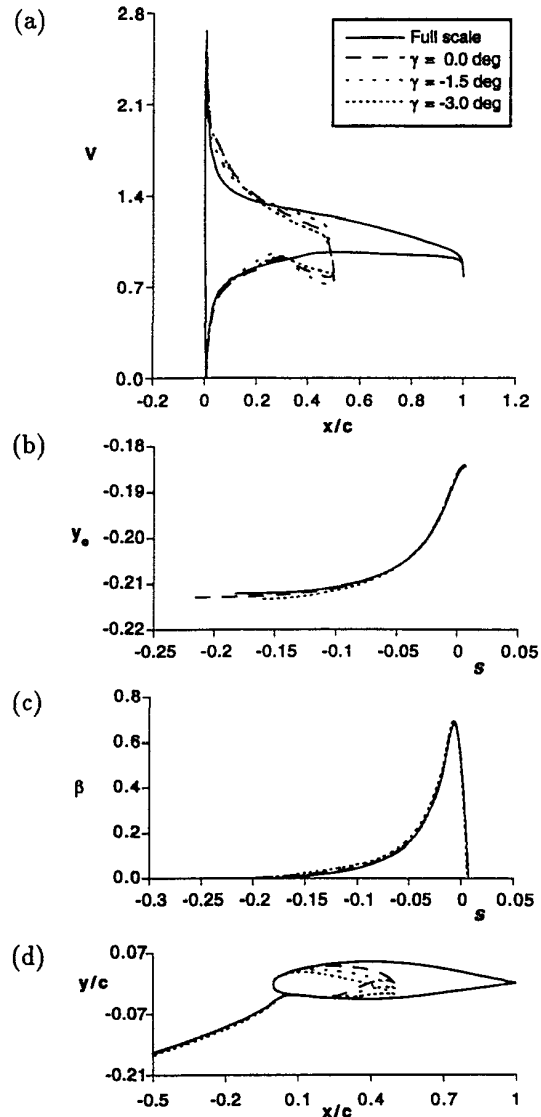


Fig. 9 Results showing (a) the velocity distribution, (b) initial displacement, (c) droplet impingement efficiency and (d) the tangent droplet trajectories at the matched conditions.

flowfield over the subscale airfoil at the design conditions.

#### Viscous Considerations

To determine the true merits of the design, a viscous flowfield analysis must form an essential part of the design. For the purpose of viscous flowfield analysis, XFOIL was utilized. XFOIL is a modified version of the ISES code<sup>19</sup> which has been successfully applied to the design and analysis of airfoils for various applications varying from human-powered aircraft<sup>20</sup> to high Reynolds number transonic transport. XFOIL utilizes a fully compatible laminar and



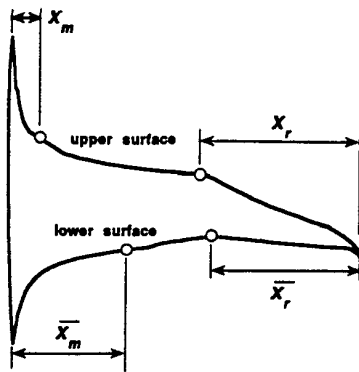


Fig. 10 The upper and lower surface match and pressure recovery locations.

turbulent viscous formulation, a reliable transition formulation and a global Newton iteration method to converge onto a flowfield solution.

The viscous analysis was performed to determine the effect of the presence of the viscous boundary on the flowfield. Typically inviscid flowfield codes over predict the airfoil lift-curve slope and the lift on an airfoil as compared to viscous flowfield codes since, in a viscous flowfield, the presence of boundary-layer decambers the airfoil and, therefore, reduces the  $C_l$ . This results in an error in the droplet trajectory calculation since at the design angle of attack, the inviscid flowfield is for a higher lift coefficient, and therefore, greater circulation. To account for this effect, a procedure called the “Matched Lift Coefficient Method” is employed, in which, the inviscid flowfield is analyzed at matched lift coefficient instead of matched angle of attack with the viscous flowfield. A brief outline of this procedure as applied to the subscale airfoil design is as follows.

Initially, the viscous  $C_{l,fs}$  is determined at the design angle of attack with the help of XFOIL. Using  $C_{l,fs}$ , an angle of attack  $\alpha_{i,fs}$  is found such that running the inviscid flowfield code at  $\alpha_{i,fs}$  produces an inviscid  $C_l$  which matches  $C_{l,fs}$ , the viscous  $C_l$ . Next, the inviscid flowfield as well as the droplet impingement characteristics of the full scale airfoil are determined at  $\alpha_{i,fs}$  and set as the target for the subscale airfoil design. A subscale airfoil is then designed to match the target flowfield and impingement characteristics. Once a match is achieved, a viscous analysis of the subscale airfoil is performed at the matched conditions to determine the viscous  $C_{l,ss}$ . As in the full scale airfoil case, an inviscid  $\alpha_{i,ss}$  is calculated and is used to determine the inviscid flowfield and droplet impingement characteristics for comparison with the target flowfield and droplet impingement characteristics. If the desired charac-

Table 3 Design Flight and Icing conditions.

Variable	Full scale	Subscale
$U$ , m/s	87	87
$T$ , deg C	-5	-5
$Re$	$6 \times 10^6$	$3 \times 10^6$
$M$	0.28	0.28
$c$ , m	1.0	0.5
$VMD$ , $\mu\text{m}$	20	20
$\alpha$ , deg	6	6
$\gamma$ , deg	0	-3
$\alpha_e$ , deg	6	9

Table 4 The converged solution.

Dependent Variables	Independent Variables
$K_S = 0.3$	$\phi_{ie} = 189.53$ deg
$c_{mo} = -0.065$	$v_1 = 2.133$
$y(x_m = 0.05)$	$\alpha^* = 8.93, 11.93, 14.93$ deg
$y(\bar{x}_m = 0.20)$	$\bar{\alpha}^* = 1.17$ deg (all segments)
$\tau = 6$ deg	$x_r = 0.0114c$ $\bar{x}_r = 0.4746c$

teristics are achieved, the design is complete, otherwise, the subscale airfoil is modified and the whole process is repeated again until the desired match is achieved.

## A DESIGN EXAMPLE

In this section, a specific design example is presented with the objective to design a half-scale model of the GLC 305 airfoil that simulates full scale droplet impingement. Table 3 lists the flight and icing conditions for the final design, whereas, Table 4 lists the final values of the design variables for the converged solution. The subscale airfoil was designed with a finite trailing-edge angle  $\tau = 6$  deg. The effects due to compressibility were also considered during the viscous flow analysis of both the airfoils.

Fig. 11 shows the comparison between the inviscid velocity distributions for the converged solution at  $\alpha_e = 6$  deg. Fig. 12 shows the comparison between the velocity distributions (viscous) at the design conditions, where,  $C_{l,fs} = 0.7690$  and  $C_{l,ss} = 0.6074$ . The respective inviscid velocity distributions for the matched lift coefficient case are shown in Fig. 13(a). All the figures show good agreement in velocity distribution over the common nose section. The comparison of the impingement characteristics corresponding to the respective matched lift coefficient cases is shown in Fig. 13(b) and (c), whereas, a comparison of tangent droplet trajectories is shown in Fig. 13(d). The results indicate excellent agreement in impingement efficiency. The tangent droplet trajectories, although originating at

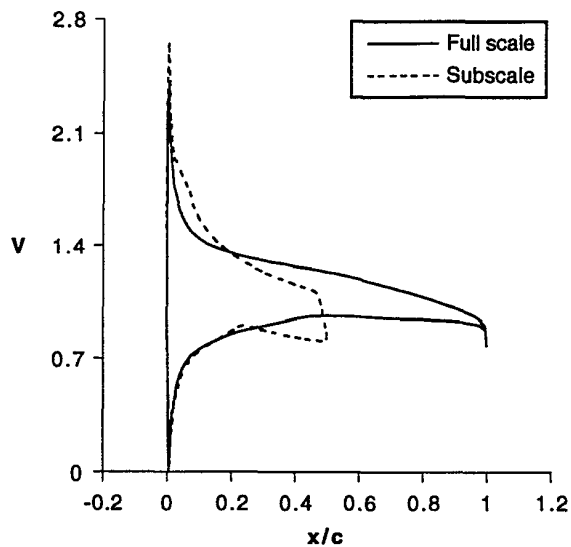


Fig. 11 Comparison between the inviscid velocity distribution at  $\alpha_e = 6$  deg.

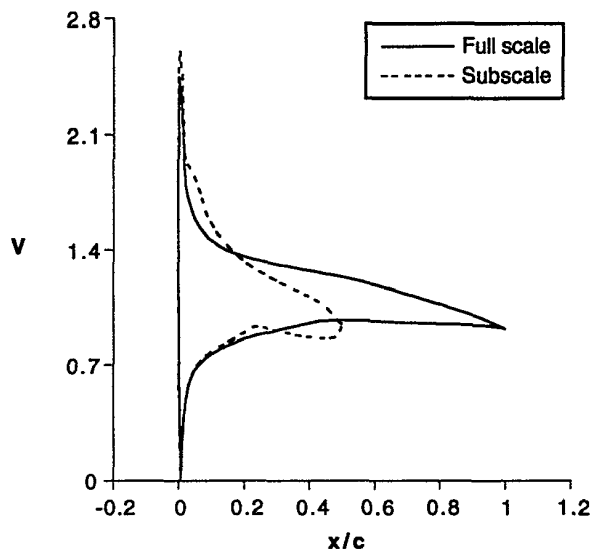


Fig. 12 Comparison between the velocity distribution at the design conditions listed in Table 3.

different locations along the y-axis, are matched in the vicinity of the leading-edge. This is consistent with the observations made during the case studies that subscale airfoils require a lower value of circulation to achieve full scale droplet impingement characteristics.

### CONCLUSIONS

Several important conclusions can be drawn from this study. First, it is shown that subscale airfoils with full-scale leading edges can be designed to exhibit full-scale droplet impingement and, there-

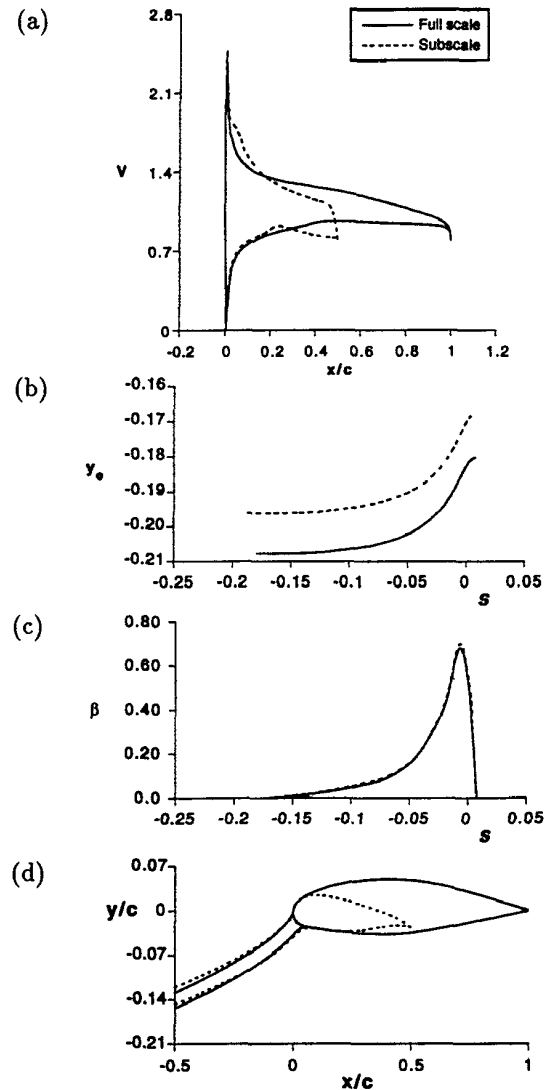


Fig. 13 Comparison between (a) the velocity distribution, (b) the initial displacement, (c) droplet impingement efficiency and (d) the tangent droplet trajectories at  $\alpha_{i,fs}$  and  $\alpha_{i,ss}$ , corresponding to the respective matched lift coefficients.

fore, ice accretion. Second, the results indicate that subscale airfoils require less circulation to simulate full scale airfoil droplet impingement characteristics. The pitching moment coefficient, of the airfoil from which the aft section for the subscale airfoil is derived, can be used effectively to achieve the desired amount of circulation on the subscale airfoil. Third, since subscale airfoils tend toward high aft-loading in order to simulate the desired droplet impingement characteristics, a nose droop can be used effectively to offset the high aft-loading. Fourth, an airfoil with

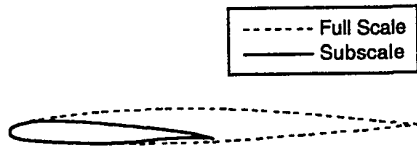


Fig. 14 The final subscale airfoil and the Learjet 305 airfoil.

a nose droop (downwards) must operate at a higher absolute angle of attack in order to keep the same angle of attack relative to its nose section as the full scale airfoil to simulate full scale impingement characteristics. Operation at high absolute angles of attack makes the subscale airfoil highly susceptible to flow separation and, therefore, it becomes necessary to integrate the viscous analysis of the flowfield over the subscale airfoil into the design process. Fifth, to incorporate viscous and compressibility effects, the "matched lift coefficient method" outlined in the paper was applied successfully in the final design example.

Although, the design method outlined in this paper is only limited to a point design, the method can be extended to a multipoint design similar in lines to the existing multipoint inverse airfoil design methods by integrating viscous boundary-layer equations and the droplet trajectory equation with the inverse airfoil design method.

### ACKNOWLEDGMENTS

This work has been sponsored by NASA Lewis Research Center under grant NCC3-408. We would like to thank Reuben Chandrasekharan of Learjet, Inc. for providing NASA Lewis with the Learjet GLC 305 airfoil used in this study. Also, helpful discussions with Tom Ratvasky, Gene Addy and Tom Bond of NASA Lewis are gratefully acknowledged.

### REFERENCES

- <sup>1</sup>Hauger, H.H., and Englar, K.G. "Analysis of Model Testing in an Icing Wind Tunnel," Rep. No. SM 14993, Douglas Aircraft Co., Inc., May 14, 1954.
- <sup>2</sup>Sibley, P.J., and Smith, R.E., Jr. "Model Testing in an Icing Wind Tunnel," Rep. No. LR 10981, Lockheed Aircraft Cor., Inc., Oct. 14, 1955.
- <sup>3</sup>Langmuir, I., and Blodgett, K., "A Mathematical Investigation of Water Droplet Trajectories," Army Air Forces TR 5418, Feb. 1946.

- <sup>4</sup>Glahn, U. H. von, "Use of Truncated Flapped Airfoils for Impingement and Icing Tests of Full-Scale Leading-Edge Sections," NACA RM E56E11, July 1956.

- <sup>5</sup>Soinne, E. and Laine, S., "An Inverse Boundary Element Method for Single Component Airfoil Design," *Journal of Aircraft*, Vol. 22, No. 6, June 1985, pp. 541-543.

- <sup>6</sup>Ormsbee, I.A. and Chen, A.W., "Multiple element Airfoils Optimized for Maximum Lift Coefficient," *AIAA Journal*, Vol. 10, No. 12, December 1972, pp. 1620-1624.

- <sup>7</sup>Kennedy, J.L. and Marsden, D.J., "A Potential Flow Design Method for Multicomponent Airfoil Sections," *Journal of Aircraft*, Vol. 15, No. 1, January 1978, pp. 47-52.

- <sup>8</sup>Eppler, R., "Direct Calculation of Airfoils from Pressure Distribution," NASA TT F-15, 417, March 1974. (Translated from *Ingenieur-Archiv*, Vol.25, No.1, 1957, pp. 32-57)

- <sup>9</sup>Eppler, R., *Airfoil Design and Data*, Springer-Verlag, New York, 1990.

- <sup>10</sup>Selig, M.S. and Maughmer, M.D., "A Multi-point Inverse Airfoil Design Method Based on Conformal Mapping," *AIAA Journal*, Vol. 30, No. 5, 1992, pp. 1162-1170.

- <sup>11</sup>Drela, M., "XFOIL: An Analysis and Design System for Low Reynolds Number Airfoils." Proceedings of the Conference on Low Reynolds Number Aerodynamics, Norte Dame, Indiana, June 1989. In *Lecture Notes in Engineering*, No. 54, Springer-Verlag, New York, pp. 1-12.

- <sup>12</sup>Bragg, M.B., "Rime Ice Accretion and Its Effect on Airfoil Performance," Ph. D. Dissertation, The Ohio State University, Columbus, Ohio, 1981.

- <sup>13</sup>Bragg, M.B., "The Effect of Geometry on Airfoil Icing Characteristics," *Journal of Aircraft*, Vol. 21, No. 7, July 1984, pp. 505-511.

- <sup>14</sup>Bragg, M.B., "A Similarity Analysis of the Droplet Trajectory Equation," *AIAA Journal*, Vol. 20, No. 12, Dec. 1982, pp. 1681-1686.

- <sup>15</sup>Ruff, A.G. and Berkowitz, "User's Manual for the NASA Lewis Ice Accretion Prediction Code (LEWICE)," NASA CR 185129, 1990.

- <sup>16</sup>Somers, D.M., "Design and Experimental Results for a Flapped Natural-Laminar-Flow Airfoil for General Aviation Application," NASA TP-1865, June 1981.

- <sup>17</sup>Maughmer, M.D., and Somers, D.M., "Design and Experimental Results for a High-Altitude, Long Endurance Airfoil," *Journal of Aircraft*, Vol. 26, No. 2, Dec. 1989, pp. 148-153.

- <sup>18</sup>Woan, C.J., "Fortran Programs for Calculating the Incompressible Potential Flow About a Single

Element Airfoil Using Conformal Mapping," The Ohio State University, Aeronautical and Astronautical Research Laboratory, TR AARL 80-02, Columbus, Ohio, January 1980.

<sup>19</sup>Drela, M., and Giles, M.B., "*ISES: A Two-Dimensional Viscous Aerodynamic Design and Analysis Code*," AIAA 87-0424, Jan. 1987.

<sup>20</sup>Drela, M., "Low-Reynolds Number Airfoil Design for the MIT Daedalus Prototype: A Case Study," *Journal of Aircraft*, Vol. 25, No. 8, Aug. 1988.